8-1-2010

Thermal History of the Ecstall Pluton from $^{40}Ar/^{39}Ar$ Geochronology and Thermal Modeling

Sarah J. Brownlee
University of California - Berkeley, sarah.brownlee@wayne.edu

Paul R. Renne
University of California - Berkeley, prenne@bgc.org

Thermal history of the Ecstall pluton from $^{40}Ar/^{39}Ar$ geochronology and thermal modeling

Sarah J. Brownlee[1] and Paul R. Renne[1,2]

1. University of California at Berkeley, Department of Earth and Planetary Science, 307 McCone Hall #4767, Berkeley, CA, 94720-4767

2. Berkeley Geochronology Center, 2455 Ridge Road, Berkeley, CA, 94704

Abstract

New $^{40}Ar/^{39}Ar$ thermochronology results and thermal modeling support the hypothesis of Hollister et al. (2004), that reheating of the mid-Cretaceous Ecstall pluton by intrusion of the Coast Mountains Batholith (CMB) was responsible for spatially variable remagnetization of the Ecstall pluton. $^{40}Ar/^{39}Ar$ cooling ages from hornblende and biotite from 12 locations along the Skeena River across the northern part of the Ecstall pluton decrease with proximity to the Quottoon plutonic complex, the nearest member of the CMB to the Ecstall pluton. The oldest $^{40}Ar/^{39}Ar$ cooling ages are found farthest from the Quottoon plutonic complex, and are 90 ± 3 Ma for hornblende, and 77.9 ± 1.2 Ma for biotite. The youngest $^{40}Ar/^{39}Ar$ cooling ages are found closest to the Quottoon plutonic complex, and are 51.6 ± 1.2 Ma for hornblende, and 45.3 ± 1.7 Ma for biotite. No obvious relationship between grain size and age is seen in the Ecstall pluton biotites. Spatial trends in $^{40}Ar/^{39}Ar$ cooling ages are consistent with model results for reheating by a thermal wall at the location of the Quottoon plutonic complex. Although no unique solution is suggested, our results indicate that the most appropriate thermal history for the Ecstall pluton includes both reheating and northeast side up tilting of the Ecstall pluton associated with intrusion of the Quottoon plutonic complex. Estimates of

northward translation from shallow paleomagnetic inclinations in the western part of the Ecstall pluton are reduced to ~3,000 km, consistent with the Baja-BC hypothesis, when northeast side up tilting is accounted for.

1. Introduction

The Baja-BC hypothesis proposes that the westernmost accreted terranes of British Columbia, which comprise the Insular and Intermontane superterranes (figure 1), accreted at low latitudes, and then translated northward up to ~3,000 km for the Insular superterrane, and ~1,100 km for the Intermontane superterrane (Umhoefer 1987, Umhoefer et al. 1997, Cowan et al. 1997). This hypothesis stems from a plethora of shallow paleomagnetic inclinations from rocks of these superterranes (Irving and Wynne, 1990). The Baja-BC hypothesis has been controversial due to a lack of supporting geologic evidence (Dickinson 1976, Davis et al. 1978, Wernicke et al. 1992) and ambiguities about the significance of the paleomagnetic data. For example Butler et al. (2006) showed that anomalously shallow paleomagnetic directions from Cretaceous plutons just west of the Ecstall pluton that crystallized at deep crustal levels, ~20 km, could be explained by crustal tilting during exhumation. In contrast, Jurassic plutons further west that crystallized at shallower crustal levels gave concordant directions with cratonic North America (Butler et al. 2006). The Ecstall pluton, an intrusive element of the Insular superterrane, is particularly interesting and controversial because it has paleomagnetic directions that change systematically from west to east. They are anomalously shallow in the west and, if taken at face value, imply poleward translation of ~7,000 km relative to North America since the mid-Cretaceous. The steeper paleomagnetic directions from the eastern part of the Ecstall pluton are concordant with results from cratonic North America. Butler et al. (2002) proposed that local scale deformation (i.e. folding) caused the anomalously shallow directions in the western Ecstall pluton, and thus that paleomagnetic directions were not consistent with large-scale northward translation. Harrison (1977) and Harrison et al. (1979) concluded that the Ecstall pluton was reheated by the Quottoon pluton resetting the ages near the Quottoon pluton. Hollister et al. (2004) went on to propose that the Ecstall pluton, and indeed the entire Insular superterrane, was reheated by intrusion and uplift of the Coast Mountains Batholith (CMB), and that reheating reset paleomagnetic directions in the Ecstall pluton by changing the thermo-chemical magnetic remanence held by lamellar magnetism in hematite-ilmenite solid solutions. Hollister et al. (2004) concluded that the steeper directions seen in the eastern part of the Ecstall pluton had been reset by the Eocene reheating, and that the shallow directions in the western Ecstall pluton were unaffected, retaining Cretaceous inclinations, and are therefore consistent with large-scale northward translation. Distinguishing between these competing hypotheses for the Ecstall pluton is critical to understanding the tectonic history of the Ecstall pluton and how it fits into the Baja-BC hypothesis.

The Coast Shear Zone (CSZ) is a large ductile shear zone that has been proposed as capable of accommodating Baja-BC-like translations (Andronicos et al. 1999). The CSZ separates the ~80-50 Ma CMB in the Intermontane superterrane from the ~91 Ma Ecstall pluton in the Insular superterrane (figure 1). A compilation of $^{40}Ar/^{39}Ar$ and K-Ar cooling ages from the Ketchikan area, which is mainly north of the Ecstall pluton, suggests that cooling ages from the Insular supperterrane are reset towards the younger CMB (Hollister et al. 2004). If reheating caused remagnetization close to the CMB, and there is no structural explanation for shallower than expected directions farther from the CMB, then large northward translation is suggested by paleomagnetic data from the Ecstall pluton.

This study uses detailed $^{40}Ar/^{39}Ar$ thermochronology on hornblende and biotite in conjunction with thermal modeling to test the reheating hypothesis for the Ecstall pluton in particular. If reheating was experienced by the entire Insular superterrane, it should be recorded by consistent spatial trends in cooling ages in the Ecstall pluton with respect to the Quottoon plutonic complex, the nearest member of the CMB. We use numerical methods, similar to those of Hollister et al. (2004), to model reheating in the crust, and find the type of thermal history that best reproduces the trends in cooling ages across the Ecstall pluton. In addition to reheating, other factors, such as exhumation history, and tilting, are considered, and prove to be important in explaining the cooling age trends found in the Ecstall pluton.

2. Methods

2.1. $^{40}Ar/^{39}Ar$ Geochronology

Hornblende and biotite were separated from 12 samples from a transect along the Skeena River (figure 2) using standard separation techniques. Crushed samples were sieved into 4 size fractions, 600-850, 450-600, 300-450, and 250-300 µm. Biotite was picked from each of the four size fractions in order to investigate possible age- grain size relationships due the effects of variable diffusion dimensions on closure temperature (e.g. Wright et al., 1991; Goodwin and Renne, 1991). Hornblende was picked from the 300-450 µm size fraction. Samples were irradiated at the OSU TRIGA reactor for 10-20 hours. Fish Canyon sanidine at 28.02 Ma (Renne et al. 1998) was used as a fluence monitor. We analyzed single grains of biotite from the largest of the two size fractions, and multi-grain aliquots of biotite from the 2 smallest size fractions, and hornblende from the 300-450 μm size fraction by step heating in 11-15 steps using a CO_2 laser. Total fusion analyses were also performed on single crystals of biotite from the small size fraction of two samples. The gas released was analyzed on a MAP 215 mass spectrometer by peak-hopping using a Balzers electron multiplier in analog mode. Because biotite age spectra produced by *in vacuo* step heating are subject to artifacts unrelated to Ar concentration gradients (e.g. Gaber et al. 1988; Lo et al. 2000; Min et al. 2001), biotite ages reported are integrated ages, calculated as the mean of all steps weighted by the amount of ^{39}Ar released in each step. For hornblende the principal concern was to obviate age bias due to biotite inclusions and thus plateau ages, generally coinciding with uniform Ca/K, were used. Though low-temperature discordance is not typical in our samples, misinterpretation of young step ages due to inclusions or secondary phases with distinct Ca/K has been shown to produce spurious conclusions about diffusive loss from hornblendes (Onstott and Peacock, 1987). A plateau as used herein includes at least 3 consecutive steps, which are mutually indistinguishable at 1-sigma and encompass 50% or more of the total ^{39}Ar released. The plateau age is calculated by the inverse variance weighted mean of all the plateau steps. Age errors are reported at the 95% confidence level.

2.2. Thermal modeling

The thermal model utilizes a finite volume approximation to the advection-diffusion equation after Patankar (1980):

$$\rho\frac{\partial\phi}{\partial t}+\rho\upsilon\nabla(\phi)=\nabla\left(D\nabla(\phi)\right)+H \tag{1}$$

where ρ = density, ϕ = heat, υ = velocity, D = diffusion coefficient, and H = heat production. Numerically we are solving the full advection-diffusion equation with a specified velocity field; however, because we have no constraints on fluid flow through the Ecstall pluton during reheating and therefore prescribe a zero velocity field, this equation can be simplified to the conduction equation:

$$\frac{\partial \phi}{\partial t} = -D\nabla^2 \phi + H \qquad (2)$$

The initial thermal structure of the crust was calculated by assuming a depth distribution of heat-producing radioactive elements. A few distributions of heat production that yield simple analytical solutions to T(y) were investigated to ensure that the numerical steady state reproduces the analytical solution (Figure 3). We chose to use the simplest distribution of heat production in the crust, i.e. constant, for further calculations because the actual distribution is unknown. The heat flux from the mantle, q_m, is held constant and chosen so that temperatures are between 250 and 300 ºC at 15 km for a given value of heat production.

We approximate the Quottoon plutonic complex as a thermal wall after Hollister et al. (2004). The thermal wall extends from 0 to 40 km depth and is 5 km thick, ~half the average width of the Quottoon plutonic complex. The boundary at the outer edge of the thermal wall, right boundary, is a zero flux boundary, approximating the center of a cooling intrusion. The left boundary is also a zero flux boundary. The surface boundary is held at 0 ºC. The lower boundary, 40 km, is held at a constant heat flux from the mantle, q_m. The effect of latent heat of crystallization is approximated by implementing an effective heat capacity during the crystallization temperature interval after Webber (1999):

(3)

$$Cp_{eff} = Cp + q_{LH} /(T_1\text{-}T_2)$$

where Cp is the heat capacity, q_{LH} is the latent heat of crystallization, and T_1-T_2 is the temperature interval over which crystallization occurs. We take T_1-T_2 to be 100 ºC (750 – 650 ºC), and q_{LH} to be 80 Cal/g. When temperatures in the thermal boundary are between 750 and 650 ºC, Cp_{eff} replaces Cp in the calculations, which lowers the thermal diffusivity and slows cooling during this interval. We prescribe an initial temperature for the thermal wall of 700 ºC, which is the temperature used for the thermal wall in Hollister et al. (2004). Care was taken to ensure that the discretization scheme led to consistent and stable results. All model parameters are listed in table 1, and a schematic illustration of the thermal model is included in electronic annex EA-1.

2.3. $^{40}Ar/^{39}Ar$ age modeling

Given a model thermal history, cooling ages are modeled by solving the diffusion equation using polar coordinates after Morton and Mayers (2005):

$$\frac{\partial C}{\partial t} = \frac{D}{r^{\alpha}} \frac{\partial}{\partial r}\left(r^{\alpha} \frac{\partial C}{\partial r} \right) + P \qquad (4)$$

where C is concentration of argon, D is the diffusion coefficient, P is production of ^{40}Ar by decay of ^{40}K, r is the radius, and α = 0, 1, or 2 for plane, cylindrical, or spherical symmetry, respectively. Biotite is modeled using cylindrical geometry, and hornblende using spherical geometry, as is generally assumed (e.g. Harrison, 1981; Grove and Harrison, 1996). We assume a zero concentration boundary at the edge of the crystal (c.f., Baxter et al., 2002). The diffusion coefficient follows the Arrhenius relationship:

$$D = D_0 \exp(E_a/RT) \qquad (5)$$

where E_a is the activation energy for argon diffusion, R is the gas constant, T is the temperature, which is obtained from the thermal model, and D_0 is the pre-exponential factor corresponding to a frequency factor of D_0/a^2, where a is the diffusion dimension. Values of E_a and D_0 are taken from Harrison (1981) for hornblende, and Grove and Harrison (1996) for biotite. Diffusion parameters for biotite may have a compositional dependence, and the composition of biotites from the Ecstall pluton varies from ~45-50% annite. For this reason model ages are calculated using both diffusion parameters from Grove and Harrison (1996), which should bracket those of the biotites from the Ecstall pluton. We assume values for effective diffusion dimension, a, of 40 μm for hornblende, which is consistent with Harrison (1981), and 500 μm for biotite, which is consistent with the largest grain dimensions, and gives reasonable closure temperatures if we are to assume that biotite retains ^{40}Ar before reheating at 15 km depth. At the start of the model, 91 Ma, we assume zero concentration of radiogenic ^{40}Ar and a uniform concentration of ^{40}K. ^{40}Ar is allowed to grow into the crystal, and diffuse out depending on the temperature, which in turn depends on location. This method of forward modeling allows us to investigate the effects of exhumation history on calculated cooling age.

3. Results

3.1 $^{40}Ar/^{39}Ar$ Geochronology

The overall trend in $^{40}Ar/^{39}Ar$ ages from the Ecstall pluton is very similar to the Hollister et al. (2004) compilation of $^{40}Ar/^{39}Ar$ and K-Ar ages for the Ketchikan region, with minor differences explained by different definitions of distance from the thermal boundary (Figure 4). In this study distance is measured to the nearest edge of the Quottoon plutonic complex, and in Hollister et al. (2004) distances are calculated by projecting sample locations onto a linear transect perpendicular to the trend of the Coast Shear Zone. Because of the different measurement techniques, the samples from Butler et al. (2002), which are from the same locations as 008, and 001 in this study, plot ~4, and ~3 km further from the thermal boundary, respectively, in the Hollister et al. (2004) compilation than in this study. In the western part of the Ecstall pluton, $^{40}Ar/^{39}Ar$ ages for hornblende are between 90 ± 3 and 79.2 ± 0.7 Ma (table 2). Biotite $^{40}Ar/^{39}Ar$ ages from this part of the Ecstall pluton are about 10 Ma younger than the hornblende cooling ages, and are between 77.9 ± 1.2 and 68.9 ± 1.1 Ma (table 2).

Closer than about 14 km from the Quottoon plutonic complex the average difference in ages between biotite and hornblende increases. This may be a result of biotite losing radiogenic ^{40}Ar by diffusion at lower temperatures than hornblende; however, age spectra remain mostly flat (Figure 5). Four size fractions of biotite were analyzed, and no clear relationship between grain size and age is seen. In many cases the smallest grain size gives the youngest age, but all size fractions are generally within error of each other (figure 4).

Hornblende from the Ecstall pluton shows evidence of reheating closer than about 8 km from the Quottoon plutonic complex with a distinct decrease in cooling ages. Hornblende age spectra commonly show evidence of minor surface-correlated excess argon in the form of anomalously old ages in low temperature heating steps (figure 6), but all yield plateaus interpreted as cooling ages. Isochrons exhibiting supra-atmospheric initial $^{40}Ar/^{36}Ar$ ratios are also indicative of excess argon (EA-2). There is no obvious spatial trend in amounts of excess argon like that observed by Baxter et al. (2002).

3.2. Modeling

When the thermal wall is set to 700 ºC at the start of the model, and then allowed to cool with latent heat release of 80 Cal/g between 750-650 ºC, the thermal structure of the crust returns to near steady state by ~20 Ma (Figures 7 and 8); however, even after 40 Ma the total energy in the system is still elevated by ~5%. Advection of heat by fluids may be an important factor that could increase cooling efficiency, however, because we have no real constraints on fluid flow through the Ecstall pluton we have ignored these effects, i.e. the model assumes that conduction controlled heat flow. This assumption is consistent with the thermal model of Hollister et al. (2004), and with the first-order observation that most of the Ecstall pluton shows little evidence of pervasive post-crystallization fluid interaction, although without a detailed isotopic study (e.g. Gordon et al. (2009)), we cannot preclude fluid interaction at the time of reheating. For the purposes of calculating model $^{40}Ar/^{39}Ar$ ages the temperatures given by the thermal model are used for 58-18 Ma (i.e. emplacement of Quottoon plutonic complex at ~58 Ma (Gehrels et al. 1991)), and the steady state geotherm is assumed for all other times.

Assuming a depth of emplacement of 27 km (7.4 – 8.4 kbar, Butler et al. 2002), a depth of reheating of 15 km as used in Hollister et al. (2004), and exhumation rates of ~0.3 km/Ma except for a 5 Ma interval (58 – 53 Ma) during and after reheating when depth is held constant, the modeled age trends are broadly consistent with the data (figure 9a) using published diffusion parameters for hornblende and biotite (table 1). The model ages are reset at approximately the same distances from the thermal boundary, and the general shape of the trend is similar for the parts of the Ecstall pluton that are clearly affected by reheating (i.e. <14 km and <8 km from the thermal boundary, for biotite, and hornblende respectively). Some misfit occurs, particularly in the distance at which hornblende ages are affected. This misfit could be reduced by a longer duration of reheating, or greater depth during reheating. Changing the initial conditions of the model, i.e. depth of emplacement, depth of reheating, and exhumation rate, all affect how accurately the model ages reproduce the measured ages, but the shape of the model age trend does not change.

4. Discussion

The age spectra for both hornblende and biotite are generally flat, even when slow cooling can be assumed, and reheating is suggested by thermal modeling. Biotite and hornblende are both hydrous minerals that are unstable during *in vacuo* laser heating, and for this reason may not produce meaningful release patterns that reflect spatial Ar isotopic gradients (e.g. Gaber et al. 1988; Grove and Harrison, 1996; Lee et al. 1991). In particular, Lee et al. 1991 suggest that breakdown of hornblende, and formation of new phases during *in vacuo* laser heating homogenizes the Ar released, and therefore it is unlikely that original spatial gradients in Ar over any one hornblende grain will be preserved. Thus, a flat age spectrum given by *in vacuo* laser heating of hornblende and biotite does not in itself preclude diffusive loss of ^{40}Ar.

The lack of a grain size effect in ^{40}Ar/^{39}Ar ages of biotite from the Ecstall pluton could be an indication that effective diffusion dimension is smaller than the smallest grain size analyzed. It could also be explained by fragments of larger grains being confused for small grain sizes. We made every effort to pick euhedral grains, but it is possible that a significant number of our small grains were actually fragments of larger grains. This could also explain why there are a few instances where single grains of approximately the same size yield ^{40}Ar/^{39}Ar ages that are not within error of each other (i.e. samples 001, Sk-9, and 008).

Agreement between the modeled and observed trends in hornblende ages might be improved if the duration of reheating is longer. Rusmore et al. (2005) showed that magmatism in the Central gneiss complex, south of our study area and just east of the Quottoon plutonic complex, was nearly continuous from 90-67 Ma, followed by rapid cooling of the entire complex at ~52 Ma. Closest to our study area, the Quottoon plutonic complex gives a U-Pb zircon age of 58.6 ± 0.8 Ma (Gehrels et al. 1991). The youngest and westernmost members of the Quottoon plutonic complex in nearby areas give ages of ~59-55 Ma, (summarized in Crawford et al. 1999). Crawford et al. (1999) conclude that the Quottoon plutonic complex was emplaced as a series of individual intrusions which would increase the duration of reheating relative to a single intrusion. Also, the timing of metamorphism in the Central Gneiss Complex indicates relatively high temperatures until ~52 Ma (Rusmore et al. 2006). An increase in the duration of reheating would increase maximum temperatures reached near the thermal boundary, and increase the distance at which hornblende $^{40}Ar/^{39}Ar$ ages are affected. It would also increase the distance at which biotite ages are affected; however, discrete intrusions would have a smaller effect at greater distances. The apparent misfit between observed and modeled age trends might also arise from lower Ar diffusivity in biotite than predicted by the experimental kinetic parameters we employed. Villa and Puxeddu (1994), for example, suggested that biotite retains argon at higher temperatures in nature than in laboratory diffusion experiments. Modeling biotite with a higher activation energy, or lower D_0, has the effect of improving the fit of modeled age trends with the observed biotite ages; however, as noted in Villa and Puxeddu (1994), the uncertainties in the temperature and duration of the reheating event are limiting factors in our ability to come to the same conclusion.

The greatest misfit between observed and modeled $^{40}Ar/^{39}Ar$ age trends occurs far from the thermal wall where cooling ages are either not affected, or only partially affected by reheating. In this region, the trend in measured cooling ages is steeper than the modeled trend, which is flat. Since this part of the Ecstall pluton is not expected to be affected by reheating according to the thermal model, there must be some other explanation for the trend in observed ages for both hornblende and biotite. One possibility is tilting after uplift through the hornblende and biotite closure isotherms. The trend in $^{40}Ar/^{39}Ar$ ages in the unheated parts of the Ecstall pluton is approximately linear for both hornblende and biotite, although there are only 3 locations beyond 14 km to constrain the trend where biotite is not expected to be affected by reheating. To explain a sloping linear trend in cooling ages by uplift and tilting, simple trigonometry leads to a relation between exhumation rate, ER, and tilt angle, ß:

$$\sin(ß) = ER*M \tag{6}$$

where M is the slope of the linear trend (see EA-3 for an illustration). This relation is true for the simplest case, where exhumation and uplift through both closure isotherms occurs before tilting. For the case when tilting and exhumation through closure isotherms are occurring simultaneously, the exhumation rate will not be constant across the tilting body, and the age relationship due to exhumation and tilting will deviate from linear. In the simplest case, for a given slope in cooling ages, greater exhumation rates imply more tilting. This relation is similar to methods using cooling histories obtained from single grains using apatite fission track modeling (Stockli et al., 2001), or multiple diffusion domain modeling on potassium feldspar (Wong and Gans, 2003) to infer pre-exhumation temperature gradients in samples from a roughly horizontal transect, indicating a depth difference between those samples prior to exhumation.

Our $^{40}Ar/^{39}Ar$ results and existing geobarometry can be used to constrain the magnitude of tilting affecting the Ecstall pluton. Differences in $^{40}Ar/^{39}Ar$ ages between hornblende and biotite at a single location unaffected by reheating provide a measure of exhumation rate if we assume the Ecstall pluton was emplaced below the biotite closure isotherm. Al-in-hornblende barometry indicates that the Ecstall pluton was emplaced at ~27-31 km depth (7.4-8.4 kbar, Butler et al. 2002), which is well below the nominal biotite closure isotherm of ~300 to 350 ˚C in most geothermal gradients, including our modeled geothermal gradient. Exhumation rates calculated using the differences in hornblende and biotite $^{40}Ar/^{39}Ar$ ages from locations unaffected by reheating, assuming emplacement below the hornblende closure isotherm and the modeled geothermal gradient, are ~0.25-1.2 km/Ma. A maximum constraint on tilting can be given by pressure estimates across the pluton. Al-in-hornblende barometry gives pressure estimates that range from 7.4-8.4 kbar across the Ecstall pluton (Butler et al. 2002). Although there is no distinct trend in pressure estimates across the Ecstall pluton, the 95% confidence limits (± ~1 kbar) allow a depth contrast of up to ~10 km across the Ecstall pluton. This constraint limits the maximum amount of tilting to ~27˚.

The effect of tilting can be easily incorporated into the diffusion model. Three scenarios, each of which changes only the timing of tilting relative to reheating, are: 1) tilt before reheating, 2) tilt after reheating, and 3) tilt occurring before, during, and after reheating (figure 7). We assume exhumation, and tilt rates, that are slow enough not to affect the geothermal gradient (i.e. no part of the Ecstall pluton is exhumed faster than ~1 km/Ma). The modeled ages match the data well when 25˚ of tilting is included (figure 9). The best fit occurs when tilting occurs before, during, and after reheating. The solution is not unique, as the length and temperature of the reheating event, as well as the structure of the Quottoon plutonic complex, and timing and rate of tilting have all been greatly simplified. However, the good fit of the model to the data suggests that $^{40}Ar/^{39}Ar$ ages in the Ecstall pluton are best explained by a thermal history that includes both reheating and tilting. Figure 10 illustrates the effects of changing uplift rate and tilt angle on the modeled cooling age trends when the tilt rate, start depth, and time of tilting (tilting is finished at 48 Ma) remain constant. Higher tilt angles and lower exhumation rates give steeper cooling age trends. If the Al-in-hornblende constraints are ignored, higher tilt angles accompanied by higher exhumation rates may produce even better agreement with $^{40}Ar/^{39}Ar$ ages (Figure 10). A consequence of tilting occurring during exhumation through closure isotherms is that uplift rates are increased towards the deeper portion of the Ecstall pluton (i.e. toward the east in this tilting scenario). The increase in uplift rates results in flattening of the modeled age trend toward the Quottoon plutonic complex, an effect that is clearest in models that omit reheating by the Quottoon plutonic complex (Figure 11). Also shown in figure 11 are the same cooling age trends when tilting occurs after uplift through both closure isotherms. These trends are straight, except for the very western part of the hornblende trend, which is already above the hornblende closure isotherm.

5. Conclusions

The trend in $^{40}Ar/^{39}Ar$ ages from the Ecstall pluton is very similar to the Hollister et al. (2004) compilation of $^{40}Ar/^{39}Ar$ and K-Ar ages for the Ketchikan region showing that the regional trend is resolved at the single pluton scale. The trends in $^{40}Ar/^{39}Ar$ ages across the Ecstall pluton are consistent with model results for reheating by the Quottoon plutonic complex. This result broadly supports Hollister et al. (2004)'s hypothesis that thermally sensitive features of the Insular superterrane, such as paleomagnetism, have been modified by intrusion of the Coast Mountains Batholith. Mineralogic changes that affect magnetic properties, and therefore the timing of acquisition of some components of remanent magnetization, have also been documented in parts of the Ecstall pluton that have been affected by reheating (Brownlee et al. 2010). This combination of results suggests that paleomagnetic data from closer than ~14 km to the Quottoon plutonic complex have been affected by reheating, and do not record ambient field conditions at the time of emplacement of the Ecstall pluton.

Model results indicate that $^{40}Ar/^{39}Ar$ cooling age trends in the Ecstall pluton are best explained by a combination of reheating and tilting. In detail, the fit of our data to specific thermal models is limited by uncertainties in diffusion parameters, including the diffusive lengthscales in the biotite and hornblende analyzed. Although a unique fit to the data is not possible without knowing more about the structure of the Quottoon plutonic complex and the timing and temperatures during emplacement of the Quottoon plutonic complex, we can constrain the maximum amount of tilting experienced by the Ecstall pluton to ~27˚ by the pressures indicated by Al-in-hornblende barometry (Butler et al. 2002). If the paleomagnetic directions from the western part of the Ecstall pluton, >14 km from the thermal boundary, are corrected for 25˚ of northeast side up tilting (tilt axis azimuth of 340˚), the northward translation implied by the shallow inclinations is substantially decreased from ~7,000 km to ~3,000 km, an estimate that is consistent with the Baja-BC hypothesis.

Trends in ^{40}Ar/^{39}Ar ages that have been affected by tilting and reheating by the Coast Mountains Batholith may be found in other plutons of the Insular superterrane that were emplaced at depths of ~20 km or more. Spatially detailed thermochronometry and thermobarometry will therefore be a necessary prerequisite to correctly interpreting paleomagnetic data from plutonic rocks in this region and critically testing the Baja-BC hypothesis.

Acknowledgements

This work was funded by NSF grant #EAR-0440029. We are grateful to Mark Harrison, Cameron Davidson, Scott Bogue, and Peter Reiners, whose careful reviews significantly improved the manuscript. We thank Lincoln Hollister for immeasurable help in conceiving the project, field work logistics, and bringing the Ecstall pluton back to life; Peter Freeman and Courtney Hart for assistance in the field; and Tim Becker for assistance in the BGC Ar lab.

References

Andronicos, C.L., Hollister, L.S., Davidson, C., and Chardon, D., 1999, Kinematics and tectonic significance of transpressive structures within the Coast Plutonic Complex, British Columbia: Journal of Structural Geology, v. 21, p. 229-243.

Baldwin, S.L., Harrison, T.M., and Fitz Gerald, J.D., 1990, Diffusion of ^{40}Ar in metamorphic hornblende: Contributions to Mineralogy and Petrology, v. 105, p. 691-703.

Baxter, E.F., DePaolo, D.J., and Renne, P.R., 2002, Spatially correlated anomalous ^{40}Ar/^{39}Ar “age” variations in biotites about a lithologic contact near Simplon Pass, Switzerland: A mechanistic explanation for “excess Ar”: Geochimica et Cosmochimica Acta, v. 66, p. 107-1083.

Brady, R.J., Ducea, M.N., Kidder, S.B., Saleeby, J.B., 2006, The distribution of radiogenic heat production as a function of depth in the Sierra Nevada Batholith, California: Lithos, v. 86, p. 229-244.

Brownlee, S.J., Feinberg, J.M., Harrison, R.J., Kasama, T., Scott, G.R., and Renne, P.R., 2010, Thermal modification of hematite-ilmenite intergrowths in the Ecstall pluton, British Columbia, Canada: American Mineralogist, in press.

Butler, R.F., Gehrels, G.E., Baldwin, S.L., 2002, Paleomagnetism and geochronology of the Ecstall pluton in the COast Mountains of British Columbia: Evidence for local deformation rather than large-scale transport: Journal of Geophysical Research, v. 107, p. 10.1029/2001JB000270.

Butler, R.F., Gehrels, G.E., Hart, W., Davidson, C., Crawford, M.L., 2006, Paleomagnetism of Late Jurassic to mid-Cretaceous plutons near Prince Rupert, British Columbia. In Haggart, J.W., Enkin, R.J, and Monger, J.W.H. (eds), *Paleogeography of the North American Cordillera: Evidence For and Against Large-Scale Displacements.* Geological Association of Canada Special Paper 46, p. 171-200.

Cowan, D.S., Brandon, M.T., Garver, J.I., 1997, Geologic tests of hypotheses for large coastwise displacements - A critique illustrated by the Baja British Columbia controversy: American Journal of Science, v. 297, p. 117-173.

Crawford, M.L., Hollister, L.S., Woodsworth, G.J., 1987, Crustal deformation and regional metamorphism across a terrane boundary, Coast Plutonic Complex, British Columbia: Tectonics, v. 6, p. 343-361.

Crawford, M.L., Klepeis, K.A., Gehrels, G., Isachsen, C., 1999, Batholith emplacement at mid-crustal levels and its exhumation within an obliquely convergent margin: Tectonophysics, v. 312, p. 57-78.

Davis, G.A., Monger, J.W.H., and Burchfiel, B.C., 1978, Mesozoic construction of the Cordilleran "collage," central British Columbia to central California, in Howell, D.G., and McDougall, K.A., ed., Mesozoic Paleogeography of the Western United States, Society of Economic Paleontologists and Mineralogists, Pacific Section, p. 1-32.

Dickinson, W.R., 1976, Sedimentary basins developed during evolution of Mesozoic-Cenozoic arc-trench system in western North America: Canadian Journal of Earth Sciences, v. 13, p. 1268-1287.

Gaber, L.J., Foland, K.A., and Corbató, C.E., 1988, On the significance of argon release from biotite and amphibole during $^{40}Ar/^{39}Ar$ vacuum heating: Geochimica et Cosmochimica Acta, v. 52, p. 2457-2465.

Gehrels, G., Rusmore, M., Woodsworth, G., Crawford, M., Andronicos, C., Hollister, L., Patchett, J., Ducea, M., Butler, R., Davidson, C., Freidman, R., Haggart, J., Mahoney, B., Crawford, W., Pearson, D., and Girardi, J., 2009, U-Th-Pb geochronology of the Coast Mountains batholith in north-coastal British Columbia: Constraints on age and tectonic evolution: Geological Society of America Bulletin, v. 121, p. 1341-1361.

Goodwin, L.B., and Renne, P.R., 1991, Effects of progressive mylonitization on Ar retention in biotites from the Santa Rosa mylonite zone, California, and thermochronologic implications: Contributions to Mineralogy and Petrology, v. 108, p. 283-297.

Gordon, S.M., Grove, M., Whitney, D.L., Schmitt, A.K., and Teyssier, C., 2009, Fluid-rock interaction in orogenic crust tracked by zircon depth profiling: Geology, v. 37, p. 735-738.

Grove, M., and Harrison, T.M., ^{40}Ar* diffusion in Fe-rich biotite: American Mineralogist, v. 81, p. 940-951.

Harrison, T.M., 1977, Fission track, Potassium-Argon, and Rubidium-Strontium geochronology and thermal history of the Coast Plutonic Complex, near Prince Rupert, B.C. B.Sc. Honors thesis, University of British Columbia, 48 pp.

Harrison, T.M., Armstrong, R.L., Naeser, C.W., and Harakal, J.E., 1979, Geochronology and thermal history of the Coast Plutonic Complex, near Prince Rupert, British Columbia.

Harrison, T.M., 1981, Diffusion of ^{40}Ar in Hornblende: Contributions to Mineralogy and Petrology, v. 78, p. 324-331.

Harrison, T.M., Duncan, I., and McDougall, I., 1985, Diffusion of ^{40}Ar in biotite: Temperature, pressure and compositional effects: Geochimica et Cosmochimica Acta, v. 49, p. 2461-2468.

Harrison, T.M., and McDougall, I. 1980, Investigation of an intrusive contact, northwest Nelson, New Zealand—II. Diffusion of radiogenic and excess ^{40}Ar in hornblende revealed by ^{40}Ar/^{39}Ar age spectrum analysis: Geochimica et Cosmochimica Acta, v. 44, p. 2005-2020.

Hollister, L.S., and Andronicos, C.L., 2006, Formation of new continental crust in Western British Columbia during transpression and transtension: Earth and Planetary Science Letters, v. 249, p. 29-38.

Hollister, L.S., Hargraves, R.B., James, T.S., Renne, P.R., 2004, The paleomagnetic effects of reheating the Ecstall pluton, British Columbia: Earth and Planetary Science Letters, v. 221, p. 397-407.

Hutchison, W.W., 1982, Geology of the Prince Rupert-Skeena map area, British Columbia: Mem. Geol. Surv. Can., v. 394, p. 116.

Irving, E., and Wynne, P.J., 1990, Paleomagnetic evidence bearing on the evolution of the Canadian Cordillera: Philosophical Transactions of the Royal Society of London, v. A331, p. 487-509.

Lee, J.K.W., Onstott, T.C., Cashman, K.V., Cumbest, R.J., and Johnson, D., 1991, Incremental heating of hornblende in vacuo: Implications for $^{40}Ar/^{39}Ar$ geochronology and the interpretation of thermal histories: Geology, v. 19, p. 872-876.

Lo, C.-H., Lee, J.K.W., Onstott, T.C., 2000, Argon release mechanisms of biotite in vacuo and the role of short-circuit diffusion and recoil: Chemical Geology, v. 165, p. 135-166.

Min, K., Renne, P.R., and Huff, W.D., 2001, $^{40}Ar/^{39}Ar$ dating of Ordovician K-bentonites in Laurentia and Baltoscandia: Earth and Planetary Science Letters, v. 185, p. 121-134.

Morton, K.W., and Mayers, D.F., 2005, Numerical Solutions of Partial Differential Equations, Cambridge University Press, 239 pages.

Onstott, T.C., Peacock, M.W., 1987, Argon Retentivity of Hornblendes - A Field Experiment in a Slowly Cooled Metamorphic Terrane: Geochimica et Cosmochimica Acta, v. 51, p. 2891-2903.

Patankar, S.V., 1980, Numerical Heat Transfer and Fluid Flow, 1st edition, Hemisphere series on computational methods in mechanics and thermal science, Taylor and Francis publisher, 214 pages.

Renne, P.R., Swisher, C.C., Deino, A.L., Karner, D.B., Owens, T.L., and DePaolo, D.J., 1998, Intercalibration of standards, absolute ages and uncertainties in $^{40}Ar/^{39}Ar$ dating: Chemical Geology, v. 145, p. 117-152.

Stockli, D.F., Linn, J.K., Walker, D., and Dumitru, T.A., 2001, Miocene unroofing of the Canyon Range during extension along the Sevier Desert Detachment, west central Utah: Tectonics, v. 20, p. 289-307.

Turcotte, D.L., and Schubert, G., 2002, Geodynamics, second edition, Cambridge University Press, 456 pages.

Umhoefer, P.J., 1987, Northward Translation of "Baja British Columbia" along the Late Cretaceous to Paleocene margin of western North America: Tectonics, v. 6, p. 377-394.

Umhoefer, P.J., Dorsey, R.J., 1997, Translation of terranes: Lessons from central Baja California, Mexico: Geology, v. 25, p. 1007-1010.

Villa, I.M., Puxeddu, M., 1994, Geochronology of the Larderello geothermal field: new data and the “closure temperature” issue: Contributions to Mineralogy and Petrology v. 115, p. 415-426.

Webber, K.L., Simmons, W.B., Falster, A.U., and Foord, E.E., 1999, Cooling rates and crystallization dynamics of shallow level pegmatitic-aplite dikes, San Diego County, CA: American Mineralogist, v. 84, p. 708-717.

Wernicke, B., and Klepacki, D.W., 1992, Escape hypothesis for the Stikine block: Geology, v. 16, p. 461-464.

Wong, M.S., Gans, P.B., 2003, Tectonic implications of early Miocene extensional unroofing of the Sierra Mazatán metamorphic core complex, Sonora, Mexico: Geology, v. 31, p. 953-956.

Wright, N., Layer, P.W., and York, D., 1991, New insights into thermal history from single grain $^{40}Ar/^{39}Ar$ analysis of biotite: Earth and Planetary Science Letters, v. 104, p. 70-79.

Figure Captions

Figure 1. Generalized geologic map of northeast British Columbia after Hollister and Andronicos (2006). The Insular superterrane is located west of the Coast Shear Zone (CSZ), and the Intermontane superterrane is located east of the CSZ. The Coast Mountains Batholith is made up of 80-50 Ma plutons and located adjacent to the CSZ in the Intermontane superterrane. The Quottoon plutonic complex is indicated by QP, and includes plutonic rocks nearest the CSZ in this view. The Ecstall pluton is outlined. Box indicates area of figure 2.

Figure 2. Generalized geologic map of the study area of the Ecstall pluton along the Skeena River near Prince Rupert, British Columbia. Sample locations are indicated by black dots, and labeled with sample names used in the text. Dashed lines a, and b are examples of how distances to the Quottoon plutonic complex were measured. Geologic

relations are after Hutchison et al. (1982), and structures are after Butler et al. (2002), and Crawford et al. (1987).

Figure 3. Geotherms produced by 3 distributions of heat production in the crust. Thick lines represent the steady state achieved by the numerical calculation, and the dashed white lines are the analytic solutions for each distribution of heat production and heat flux from the mantle, q_m, which can be found in Turcotte and Schubert (2002). The black curve is the steady state geotherm used in the modeling. Also shown are the closure temperature ranges for biotite and hornblende calculated using diffusion parameters from table 1, and cooling rates of 1 and 20 ºC/Ma. The modeled depths of the Ecstall pluton during emplacement and reheating are also shown.

Figure 4. $^{40}Ar/^{39}Ar$ results from this study (diamonds) and the compilation of $^{40}Ar/^{39}Ar$ and K-Ar results from the Ketchikan region of Hollister et al. (2004), (circles and squares). As discussed in the text, the square symbols are samples 008, and 001, from Butler et al. (2002), which are from the same locations as 008, and 001 in this study, but they plot ~4 and ~3 km further from the thermal boundary due to the different methods of measuring distance to the thermal boundary used in this study vs. Hollister et al. (2004). The inset shows only results from this study. For samples from this study, symbol size corresponds to grain size fraction analyzed. The gray error bars are 2σ.

Figure 5. Representative biotite age spectra from three samples, 008, 001, and Sk-5 at 21.1 km, 6.8 km, and 3.9 km from the thermal boundary, respectively. Single grain and multi-grain examples are shown.

Figure 6. Representative hornblende age spectra from >14 km, 14-8 km, and <8 km from the thermal boundary.

Figure 7. Thermal model results at 91, 58, 53, and 18 Ma. Lines a, b, c, and d are the locations of sample transects for 4 different scenarios of exhumation and tilt.

Figure 8. Thermal model results at the depth of reheating, 15 km. a) Temperature vs. distance from the Quottoon plutonic complex at 10,000 a, 1, 5, 10, and 40 Ma after reheating (after 58 Ma). b) Temperature vs. time at the center of the thermal boundary (-5 km), and 0.5, 5, 10, 15, 20, and 25 km from the edge of the thermal boundary. Hornblende and biotite closure temperatures calculated from diffusion parameters in table 1 and using 1 and 20 ºC/Ma cooling rates are shown.

Figure 9. ^{40}Ar/^{39}Ar ages and model age trends for the 4 uplift and tilt scenarios in figure 7 plotted vs. distance from the Quottoon plutonic complex. black diamonds- hornblende, white diamonds- biotite. Symbol size corresponds to grain size fraction analyzed. Diffusion parameters used in the model are from Harrison (1981) for hornblende, and Grove and Harrison (1996) for biotite. Model cooling age trends are shown as solid lines (black- hornblende, gray- biotite) with dashed lines representing the ages calculated using diffusion parameters plus or minus their reported errors. For hornblende the diffusion parameters plus reported error plots on top of the solid line. a) no tilt, b) tilt before reheating, c) tilt after reheating, and d) tilt before, during, and after reheating.

Figure 10. Model results for a variety of exhumation rates and tilt angles. The position during reheating is the same for all models. This is achieved by stopping exhumation once the reheating depth is reached, which results in holding the deeper, and more eastern parts of the Ecstall pluton in the biotite partial retention zone for longer periods when higher exhumation rates are assumed. For all, the tilt rate is 1˚/Ma, and tilting ends at 48 Ma (10 Ma after the start of reheating), thus tilting begins earlier for higher tilt angles.

Figure 11. Model results when reheating is not included. When tilting occurs during uplift through closure isotherms, the age trends flatten toward the east as exhumation rates are increased due to tilting. The effect of holding the deeper parts of the Ecstall pluton in the biotite partial retention zone is seen by a steepening of the biotite model age trend at ~14 km when 0.4 km/Ma exhumation rate is assumed. When tilting occurs only after exhumation of the entire pluton through both closure isotherms (i.e. constant exhumation rate until entire pluton is above ~15 km depth, followed by tilting), the age trends are straight lines, as predicted by the relation between exhumation rate, tilt angle, and slope of the age trend.

Table 1. Model parameters used for the thermal model and the diffusion/ age model. Thermal model parameters were chosen to be similar to Hollister et al. (2004). Diffusion parameters are from (a) Harrison, 1981, (b) Grove and Harrison, 1996.

Table 2. $^{40}Ar/^{39}Ar$ results. Errors are 2σ. Data from individual steps can be found in the electronic annex.

Thermal model parameters	
Total width	50 km
Total depth	40 km
Grid spacing (dx, and dy)	0.5 km
Total duration	40 Ma
Time step	10,000 yr
Density (ρ)	2,700 g/cm^3
Heat capacity (c)	1100 kJ/˚C
Thermal conductivity (K)	2.5 mW/km ˚C
Heat production (H)	1.0 µW/m^3
Latent heat production (q)	80 Cal/g
Latent heat interval (T_1-T_2)	100 ˚C (750-650 ˚C)
Heat flux in from mantle (f_m)	20 mW/km^2
Temperature at surface	0 ˚C
Temperature at thermal wall	700 ˚C
Thickness of thermal wall	5 km

Diffusion model parameters	Hornblende	Biotite
Total duration	91 Ma	91 Ma
Time step	65,000 yr	65,000 yr
^{40}K decay constant	5.543 e-10 /yr	5.543 e-10 /yr
Branching ratio	0.117	0.117
Grain size radius (r)	250 µm	250 µm
Grid spacing (dr)	10 µm	10 µm
Geometry	Sphere	Cylinder
Diffusion parameters		
Activation energy 1 (Ea)	64.1 ± 1.7 kcal/mol (a)	47.1 ± 1.5 kcal/mol (b)
Preexponential factor 1 (d_0)	0.024 +/- 0.053/0.011 cm^2/s (a)	0.075 +/- 0.97/0.042 cm^2/s (b)
Activation energy 2 (Ea)		50.5 ± 2.2 kcal/mol (b)
Preexponential factor 2 (d_0)		0.403 +/- 0.933/0.282 cm^2/s (b)
Effective diffusion dimension (a)	40 µm	500 µm

Table 1.

Hornblende step heating results							
Sample	Grain size (µm)	Distance from Quottoon Pluton (km)	Plateau age (Ma)	Integrated age (Ma)	MSWD	P	# of steps in plateau
Sk-4A	300-425	3.5	51.6 ± 1.2	51.7 ± 0.9	2.21	0.01	all
Sk-5A	250-425	3.9	54.4 ± 0.5	55.0 ± 0.7	1.68	0.15	5 of 10
Sk-6A	300-425	5.9	55.4 ± 1.1	55.2 ± 0.6	2.8	0.01	7 of 11
Sk-7A	300-425	6.1	57.1 ± 1.7	57.3 ± 0.8	3.19	0	10 of 11
Sk-8B	300-425	6.3	57.4 ± 1.3	62.1 ± 1.7	1.14	0.33	4 of 11
OO1	300-425	6.8	70.5 ± 1.1	66.5 ± 1.0	1	0.44	13 of 14
OO1	250-425	6.8	67 ± 2	68.5 ± 1.2	2.24	0.05	6 of 14
Sk-10B	425-600	7.6	68 ± 2	71.6 ± 1.5	3.63	0.01	5 of 11
Sk-10B	250-300	7.6	69.5 ± 1.2	70.1 ± 1.3	0.61	0.79	10 of 11
Sk-9A	250-425	10.6	75.9 ± 0.7	77.1 ± 0.8	1.27	0.24	11 of 12
Sk-9B	300-425	10.6	77.3 ± 0.7	78 ± 0.8	0.78	0.65	11 of 12
Sk-3A	300-425	13.4	79.3 ± 0.6	79.5 ± 0.8	1.28	0.23	11 of 12
Sk-2A	300-425	16.4	83.4 ± 1.2	83.7 ± 1.3	1.03	0.41	11 of 12
Sk-1A	300-425	17.3	83.1 ± 1.7	83 ± 1.3	1.85	0.05	11 of 12
Sk-1A	250-425	17.3	79.2 ± 0.7	78.3 ± 0.8	0.94	0.46	6 of 12
OO8	300-425	20.1	83.1 ± 1.3	83.8 ± 1.4	1.68	0.08	11 of 12
OO8	250-425	20.1	85.7 ± 1.1	86.6 ± 1.3	0.51	0.88	10 of 13
OO8	250-425	20.1	90 ± 3	92 ± 2	2	0.04	10 of 12

Biotite step heating results							
Sample	grain size (µm)	Distance from Quottoon Pluton (km)	Integrated age (Ma)	Plateau age (Ma)	MSWD	P	# of steps in plateau
Sk-5A	425-850	3.9	47.1 ± 0.8	47.2 ± 0.7	0.64	0.78	all
Sk-5A	425-850	3.9	47.7 ± 1.0	47.8 ± 0.8	0.21	1	all
Sk-5A	250-425	3.9	46.2 ± 1.5	46.6 ± 1.3	0.53	0.87	all
Sk-6A	600-850	5.9	46.5 ± 1.2	47.3 ± 1.0	0.94	0.49	all
Sk-6A	600-850	5.9	47.9 ± 0.9	47.7 ± 0.7	0.48	0.92	all
Sk-6A	425-600	5.9	46 ± 2	47.1 ± 1.6	0.49	0.89	all
Sk-6A	425-600	5.9	48.2 ± 1.1	47.8 ± 0.7	0.83	0.61	all
Sk-6A	300-425	5.9	48.1 ± 0.6	48.4 ± 0.5	0.6	0.8	10 of 13
Sk-6A	250-300	5.9	48.1 ± 0.6	48.2 ± 0.5	1.68	0.08	11 of 13
Sk-7A	300-425	6.1	45.3 ± 1.7	47 ± 5	2.72	0	all
Sk-7A	300-425	6.1	50 ± 2	48.8 ± 1.6	0.23	0.99	all
Sk-7A	300-425	6.1	48.2 ± 0.6	48.7 ± 0.5	1.44	0.16	11 of 13
Sk-7A	250-300	6.1	48 ± 0.6	49.1 ± 0.6	1.74	0.07	10 of 13
Sk-8B	300-425	6.3	48.6 ± 0.9	50.7 ± 0.9	0.81	0.6	9 of 13
OO1	600-850	6.8	56.8 ± 1.0	58.1 ± 1.0	1.91	0.07	7 of 11
OO1	600-850	6.8	52 ± 1.1	51.7 ± 0.9	0.54	0.89	all
OO1	425-600	6.8	50.1 ± 1.6	50.2 ± 1.3	0.21	1	all
OO1	425-600	6.8	49.9 ± 1.6	51.3 ± 1.0	2.46	0.06	3 of 11
OO1	300-425	6.8	52.2 ± 0.8	52.4 ± 0.8	0.86	0.58	12 of 13
OO1	250-300	6.8	51.5 ± 0.8	51.6 ± 0.8	0.73	0.71	12 of 13
OO1	425-850	6.8	53.1 ± 0.7	53.1 ± 0.6	0.57	0.93	all
OO1	250-425	6.8	54.3 ± 1.5	54.3 ± 1.3	0.44	0.95	all
Sk-9A	425-850	10.6	56.5 ± 0.6	56.7 ± 0.5	1.4	0.17	all
Sk-9A	425-850	10.6	59.1 ± 0.6	59.2 ± 0.5	0.67	0.75	all
Sk-9A	250-425	10.6	55 ± 1.3	55.1 ± 1.1	0.28	0.99	all
Sk-9B	300-425	10.6	55.5 ± 0.6	55.9 ± 0.5	0.52	0.84	9 of 11
Sk-9B	250-300	10.6	55.5 ± 0.6	55.8 ± 0.5	1.51	0.15	9 of 11
Sk-9B	600-850	10.6	58.3 ± 1.0	59.6 ± 0.8	1.64	0.13	7 of 11
Sk-9B	600-850	10.6	58.2 ± 0.5	58.3 ± 0.4	0.93	0.52	all
Sk-9B	425-600	10.6	58.6 ± 1.5	59.1 ± 1.0	0.6	0.86	all

Biotite step heating results cont'd…							
Sample	grain size (µm)	Distance from Quottoon Pluton (km)	Integrated age (Ma)	Plateau age (Ma)	MSWD	P	# of steps in plateau
Sk-3A	300-425	13.4	64.5 ± 0.7	67.4 ± 1.8	2.36	0.02	8 of 11
Sk-3A	250-300	13.4	61.9 ± 0.9	64.4 ± 0.8	0.61	0.75	8 of 11
Sk-3A	600-850	13.4	62 ± 0.8	62 ± 2	3.08	0.01	6 of 14
Sk-3A	600-850	13.4	66.7 ± 0.8	68.1 ± 0.6	1.45	0.2	6 of 11
Sk-2A	300-425	16.4	68.9 ± 1.1	70.1 ± 1.4	2.3	0.02	8 of 11
Sk-2A	250-300	16.4	68.0 ± 1.1	69.6 ± 1.0	0.85	0.54	8 of 11
Sk-2A	600-850	16.4	70.0 ± 1.1	71.9 ± 2	3.79	0	6 of 11
Sk-2A	425-600	16.4	68.9 ± 1.1	69.3 ± 1.1	1.03	0.41	9 of 11
Sk-1A	300-425	17.3	73.0 ± 1.1	74.3 ± 1.6	2.31	0.02	8 of 11
Sk-1A	250-300	17.3	73.5 ± 1.2	75.5 ± 1.2	0.22	0.98	8 of 11
Sk-1A	600-850	17.3	70.3 ± 1.1	70.3 ± 1.8	3.34	0	9 of 11
Sk-1A	600-850	17.3	75.2 ± 1.6	75.1 ± 1.4	0.24	0.99	all
Sk-1A	600-850	17.3	75.6 ± 1.6	75.8 ± 1.4	0.74	0.72	all
Sk-1A	425-600	17.3	75.0 ± 1.4	75.4 ± 1.3	1.22	0.27	all
Sk-1A	425-850	17.3	76.8 ± 0.9	77.2 ± 0.8	0.4	0.92	9 of 11
Sk-1A	425-850	17.3	74.0 ± 0.8	74.3 ± 0.7	0.85	0.56	9 of 11
Sk-1A	250-425	17.3	70.6 ± 1.2	72 ± 1.1	0.23	0.98	8 of 11
OO8	300-425	20.1	76.0 ± 1.2	76.1 ± 1.2	0.67	0.75	all
OO8	250-300	20.1	75.8 ± 1.2	75.9 ± 1.1	1.65	0.08	10 of 11
OO8	600-850	20.1	73.8 ± 1.4	73.6 ± 1.2	0.48	0.9	all
OO8	600-850	20.1	77.4 ± 1.2	77.3 ± 1.2	1.07	0.38	all
OO8	425-600	20.1	74.9 ± 1.4	75.8 ± 1.2	1.77	0.06	all
OO8	425-600	20.1	75.7 ± 1.7	76 ± 1.5	0.29	0.99	all
OO8	250-425	20.1	77.4 ± 1.5	77.2 ± 1.2	1.34	0.18	all
OO8	425-850	20.1	77.9 ± 1.2	78.0 ± 0.9	1.16	0.28	all

Biotite total fusion results						
Sample	Grain size (µm)	Distance from Quottoon Pluton (km)	Total fusion age (Ma)	Weighted mean (Ma)	MSWD	p
OO1	250-425	6.8	51.9 ± 0.4			
OO1	250-425	6.8	51.6 ± 0.4			
OO1	250-425	6.8	53 ± 0.7			
OO1	250-425	6.8	53.2 ± 0.7			
OO1	250-425	6.8	52.2 ± 0.7	52 ± 1	2.21	0.02
OO1	250-425	6.8	52.6 ± 1.6			
OO1	250-425	6.8	52.2 ± 0.5			
OO1	250-425	6.8	52.3 ± 0.4			
OO1	250-425	6.8	52.4 ± 0.5			
OO1	250-425	6.8	52.5 ± 0.4			
OO8	250-425	20.1	75 ± 0.6			
OO8	250-425	20.1	77.2 ± 0.7			
OO8	250-425	20.1	75.3 ± 0.6			
OO8	250-425	20.1	76.1 ± 0.6			
OO8	250-425	20.1	76.7 ± 0.6	76.3 ± 1.6	5.12	0
OO8	250-425	20.1	76.3 ± 0.7			
OO8	250-425	20.1	77.5 ± 0.5			
OO8	250-425	20.1	75.6 ± 0.5			
OO8	250-425	20.1	76.8 ± 0.6			
OO8	250-425	20.1	77.4 ± 0.6			

Table 2.

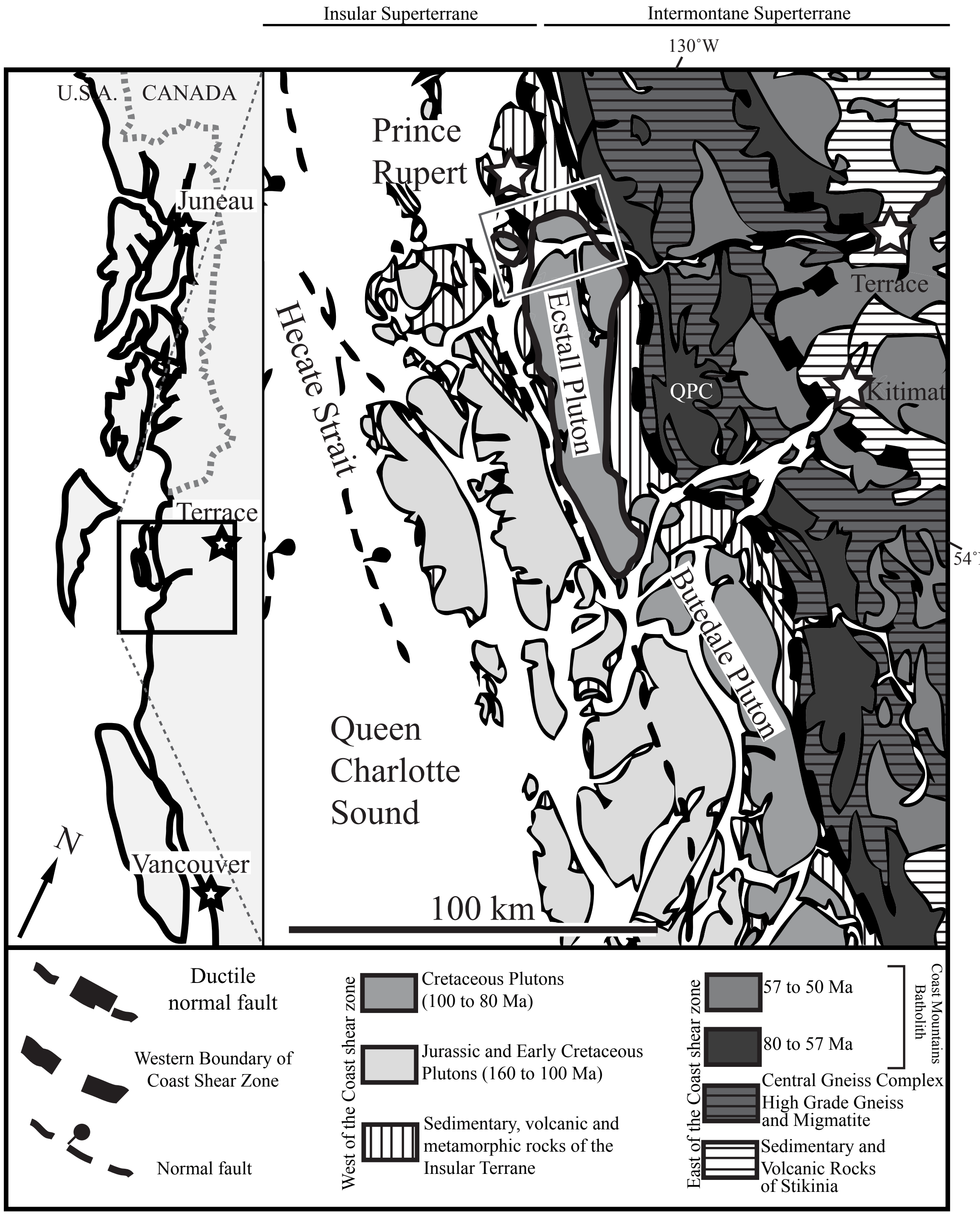

Brownlee and Renne, Figure 1

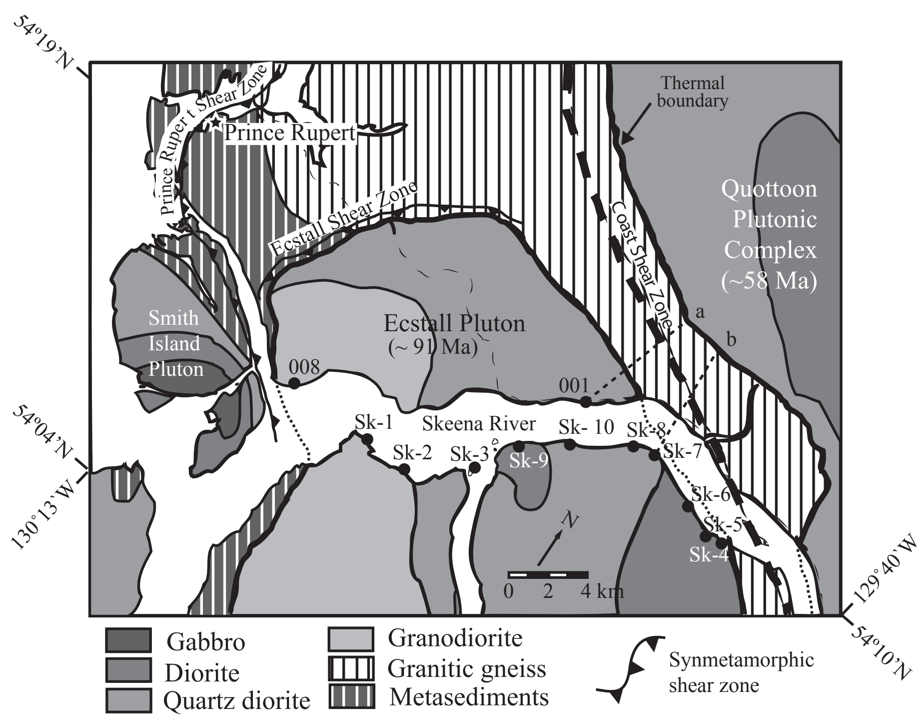

Brownlee and Renne, Figure 2

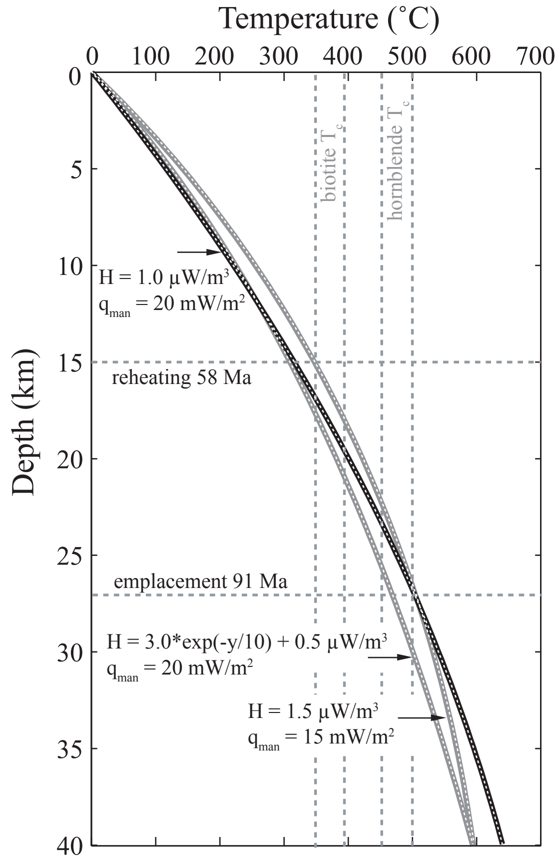

Brownlee and Renne, Figure 3

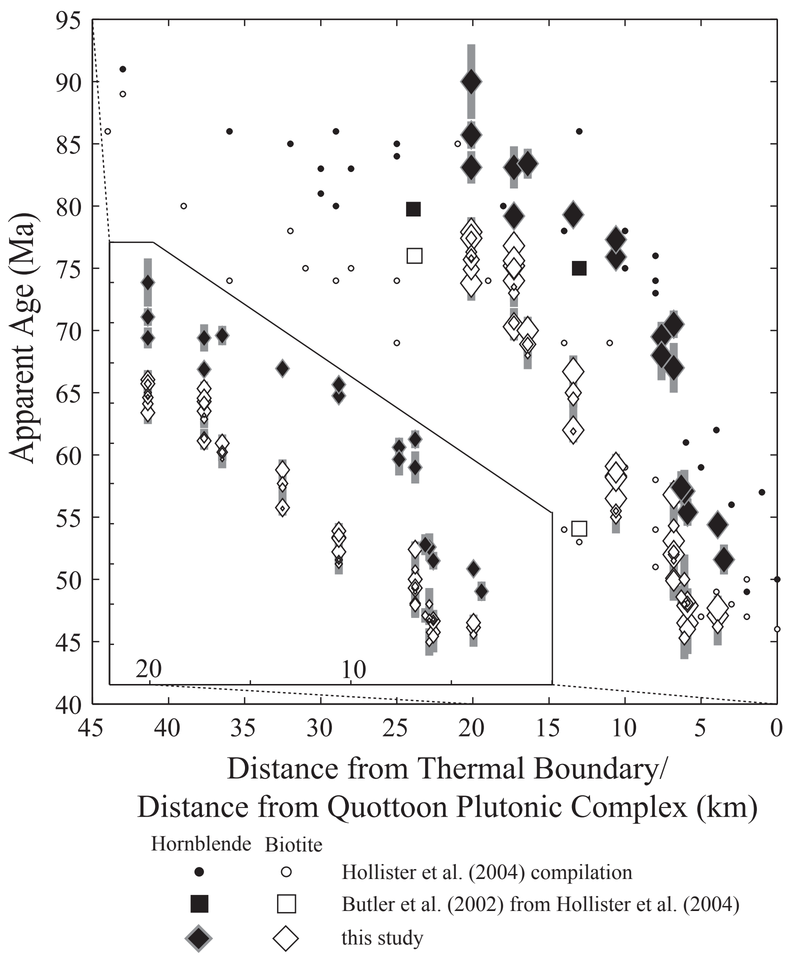

Brownlee and Renne, Figure 4

Biotite Age Spectra

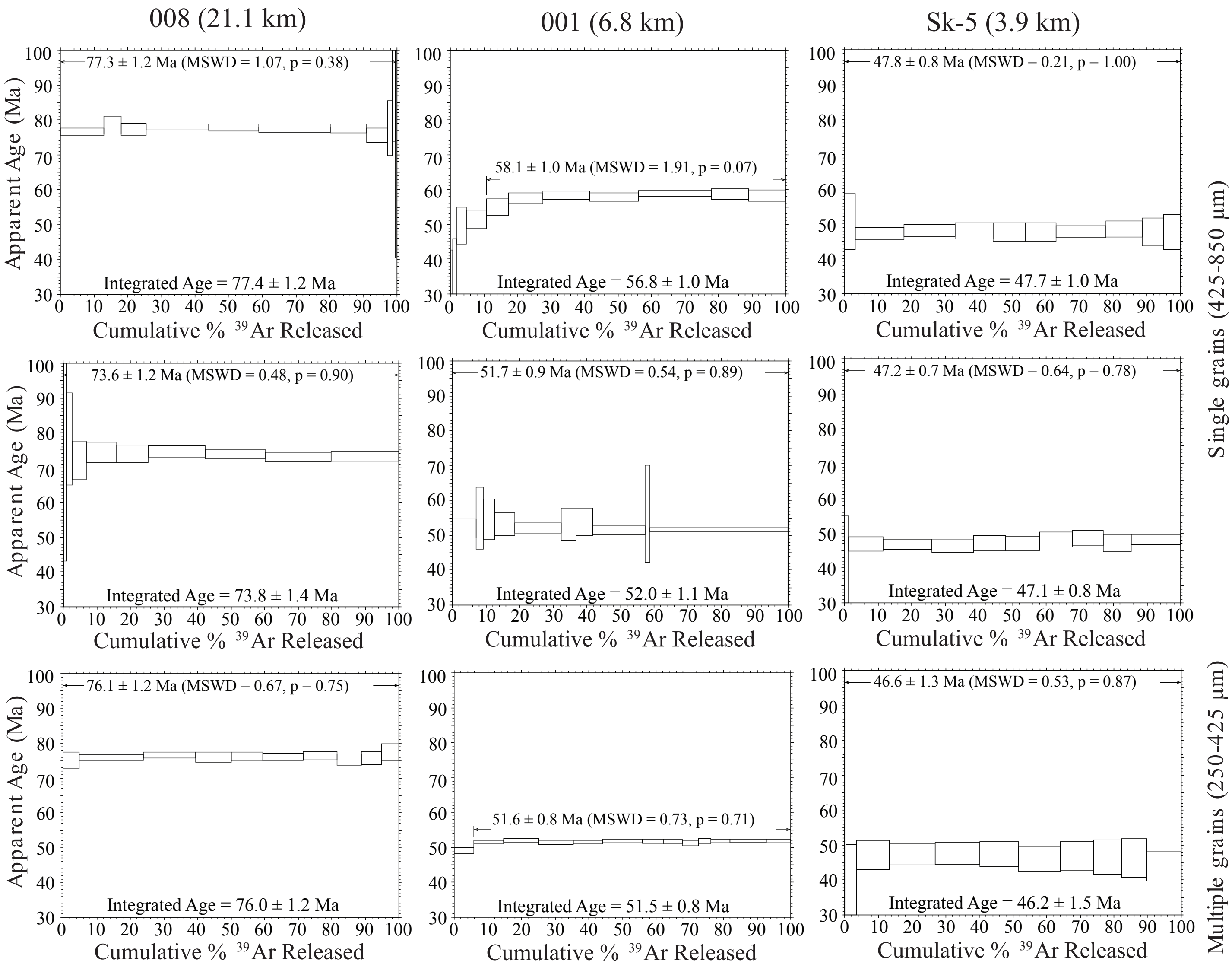

Brownlee et al. Figure 5

Hornblende Age Spectra

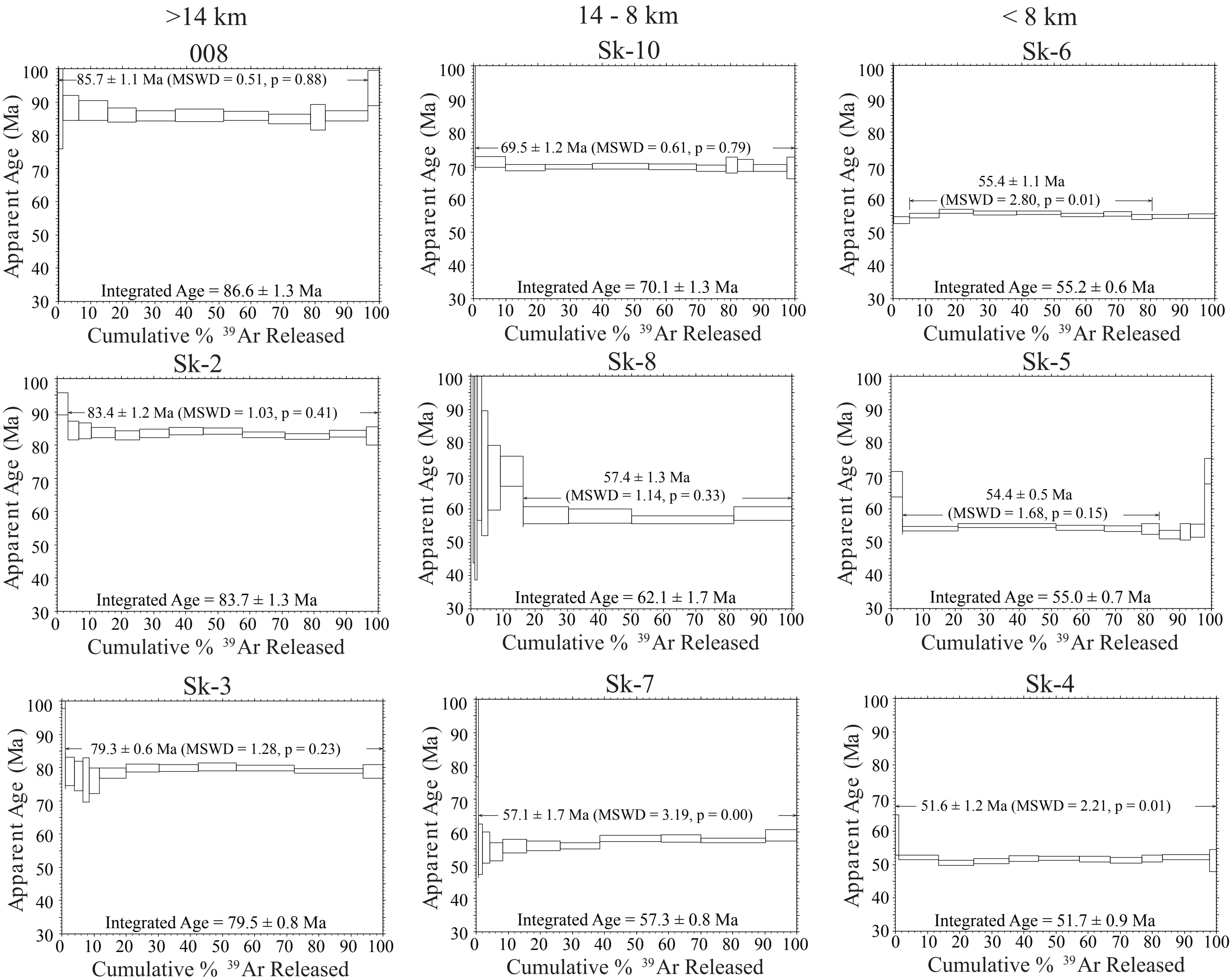

Brownlee et al. Figure 6

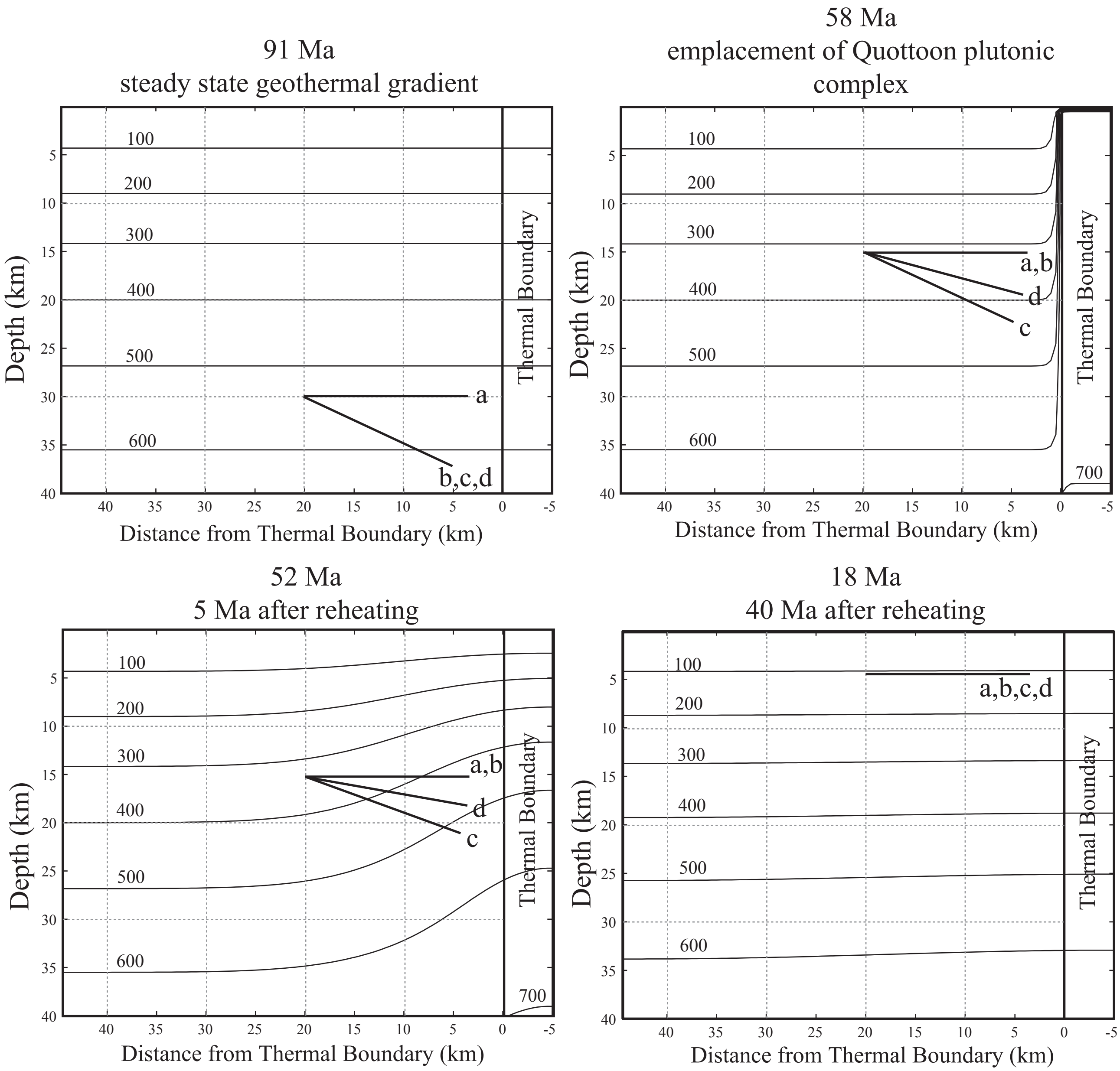

Brownlee and Renne, Figure 7

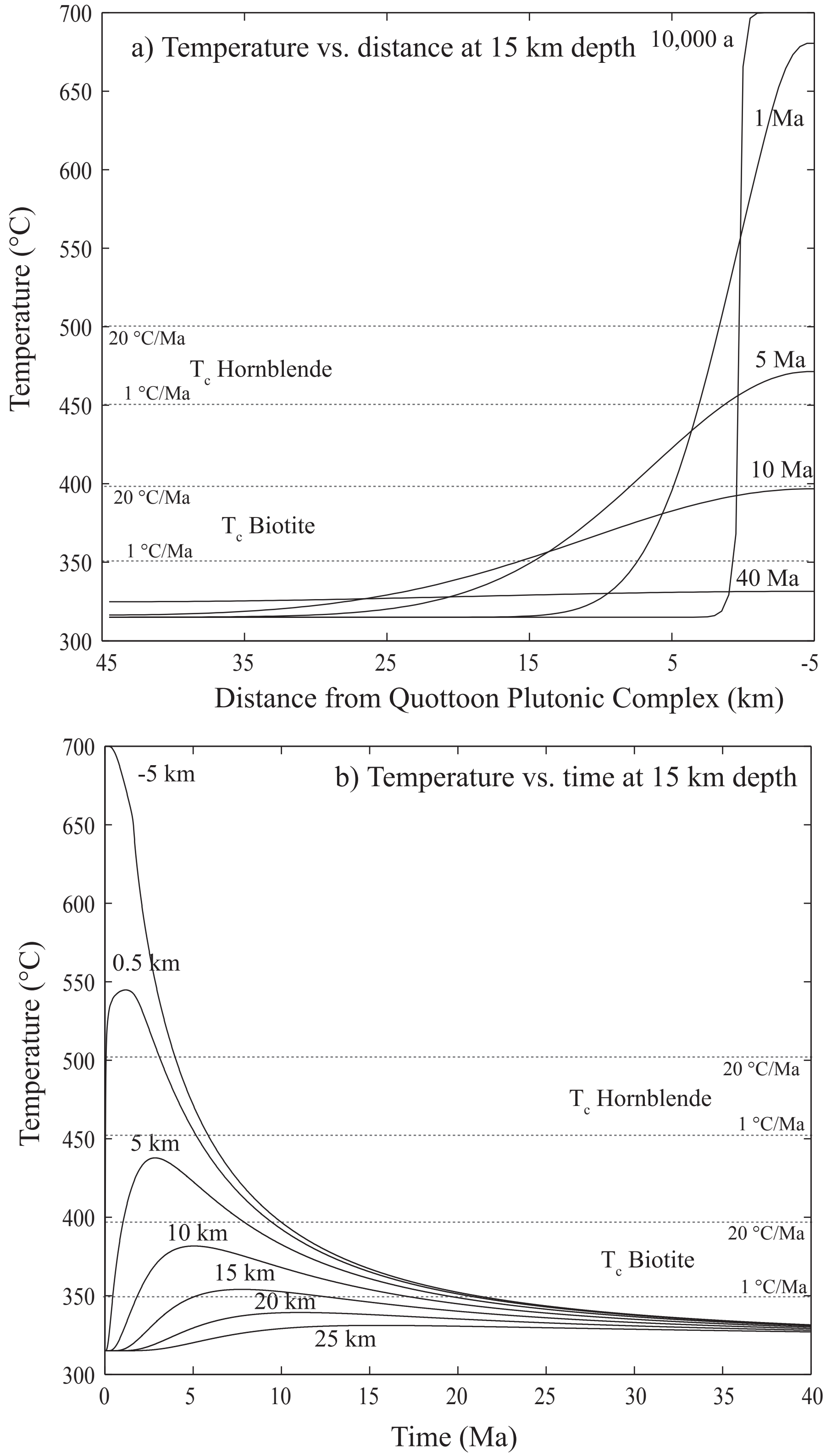

Brownlee and Renne, Figure 8

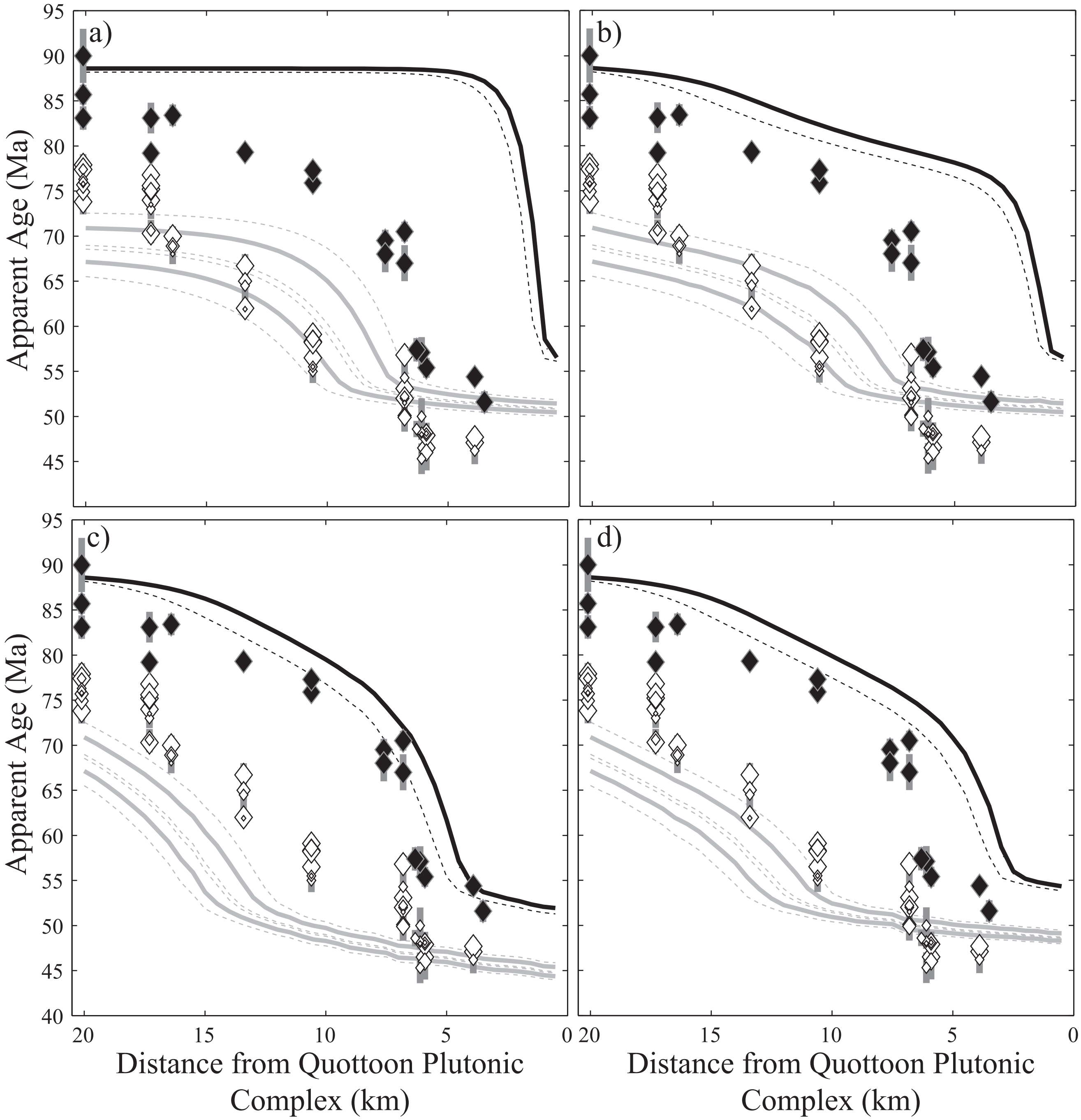

Brownlee and Renne, Figure 9

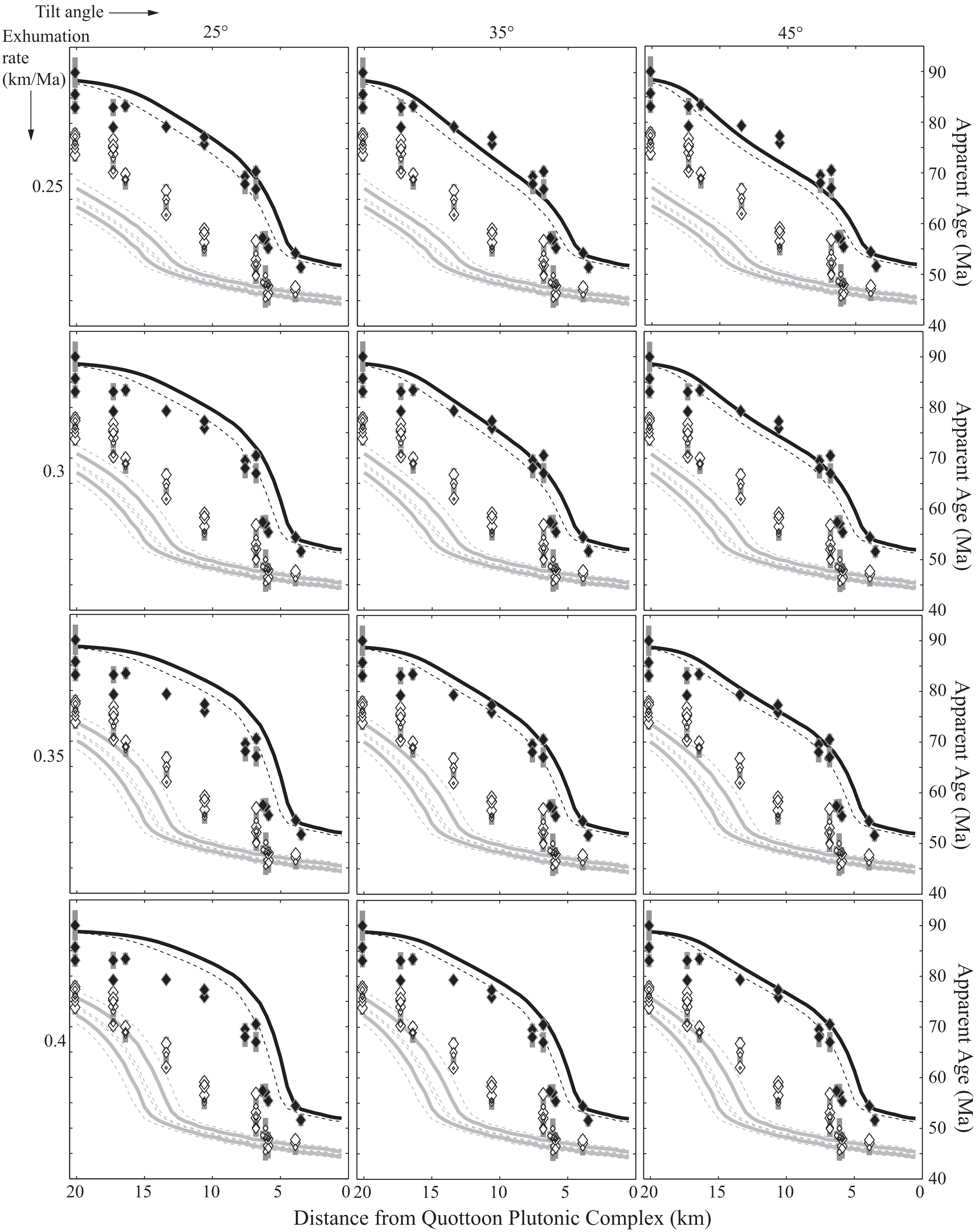

Brownlee and Renne, Figure 10

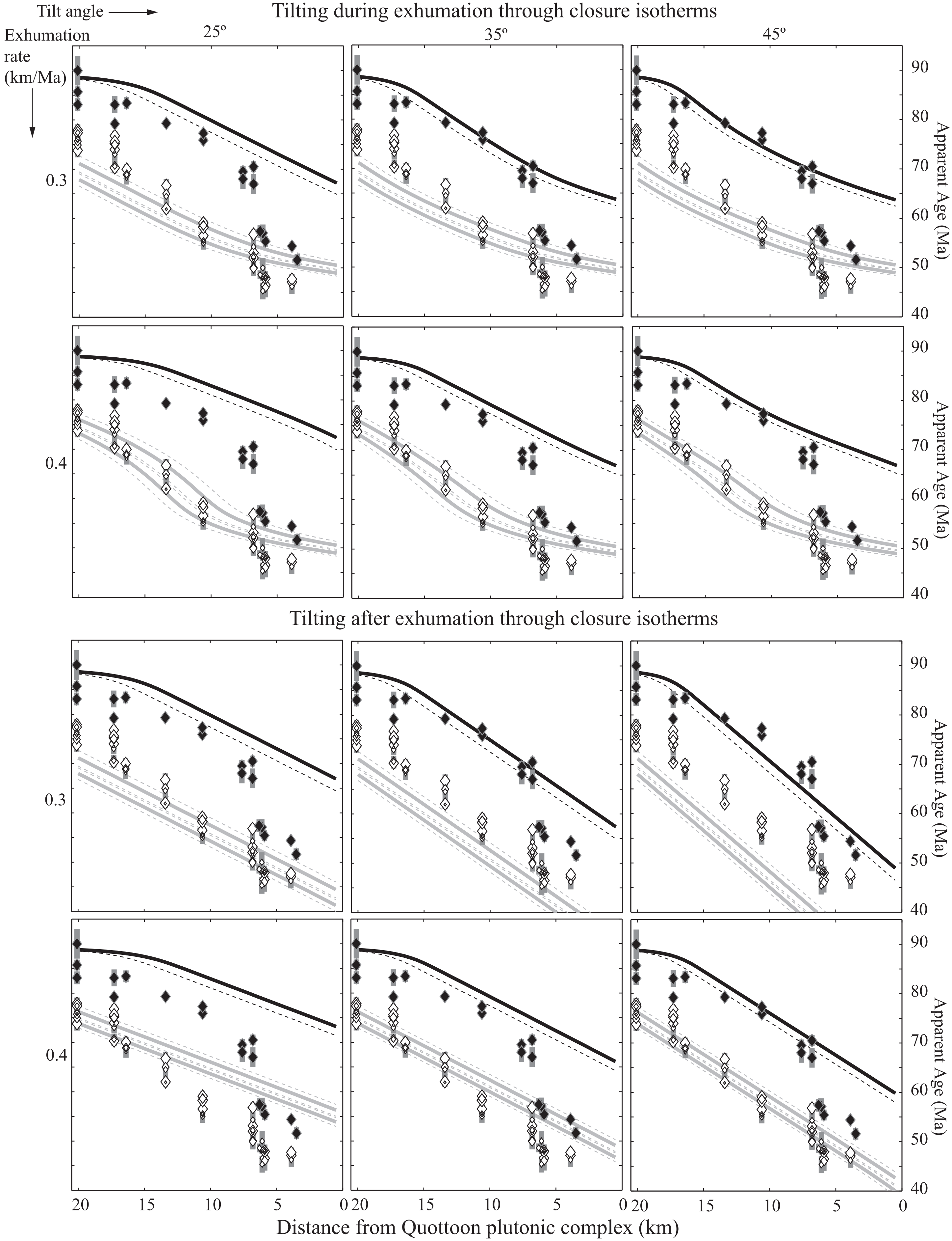

Brownlee and Renne, Figure 11